CHAPTER-4

Electrochemical Fe(III) ion Incorporation in the Structure of ZIF-67- Derived Co-Layered Double Hydroxide Boosts Water Oxidation Activity

In this chapter, we have demonstrated the electrochemical reconstruction of ZIF-67 during anodic water oxidation, resulting in the formation of FeCo-LDH-x. During this process, Fe(III) ions from the electrolyte solution are incorporated into the structure of the active catalyst. The electrochemically derived FeCo-LDH-3 exhibited a high electrochemical surface area, numerous exposed active sites, atomic-level thickness, and optimized structural and electronic features, all of which enhance its OER activity. All FeCo-LDH-x catalysts demonstrated superior activity compared to the as-synthesized Co-LDH-3. Of these, FeCo-LDH-3 showed the highest OER activity, generating a current density of 50 mA cm^{-2} at an overpotential of 180 mV, and exhibited the lowest Tafel slope value and charge transfer resistance.

4.1. Introduction

MOFs undergo structural reconstruction following phase transition, structural reorganization, morphological modifications, and compositional adjustment under anodic potential to form active catalyst $M(OH)_2$-M(O)-$(OH)_y$.[1][2][3][4] The ultrathin nanosheets of active catalyst produced by the electrochemical transformation provide a number of advantages:[5][6][7] i) there is no need of high temperature and pressure for the transformation, ii) electrochemical synthesis produces ultrathin nanosheets with an extremely high and scalable yield,[8][9] iii) the $M(OH)_{2-}M(O)_{x(}OH)_y$ ultrathin nanosheets exhibit an ideal inter-layer spacing,[10][11] iv) this method produces ultrathin nanosheets with uniform and atomic level thickness v) under applied anodic potential, the catalytically active metal centers in ultrathin nanosheets undergo oxidation and attain higher oxidation state 3+/4+ to form $M^{3+}OOH$ and $M^{4+}OO^-$ leading to the facile formation of O-O.[2][12][13][14][15][16][17]

In this context, Tian et al. developed Co-oxyhydroxides nanosheets by electric-field assisted hydrolysis of FJI-H25FeCo-MOF which required only 230 mV of overpotential to produce current density of 10 mA cm^{-2} with long term stability for 30 h.[18] Further, Ling et al. synthesized $Fe_{0.67}Co_{0.33}OOH$ by electrochemical reconstruction of Fe_2Co-MIL-88B MOF. As synthesized catalyst exhibited 230 mV overpotential for 10 mA cm^{-2} current density along with stability for 50 h.[19] Our group also reported the improvement in OER activity of NiOOH by incorporation of high valent V during electrochemical reconstruction of Ni-coordination polymer.[17] Electrochemical reconstruction of CoFeCo-PBA into the active catalyst was also found to improve the OER activity.[20]

Recently, Li et al. developed amorphous and defect rich metal hydroxide by electrochemical reconstruction of ZIF-L/NF embedded with rich oxygen vacancy, high conductivity and short diffusion path. As obtained catalyst $Co(OH)_2$-ZIF-L/NF-y exhibited excellent OER activity. [21]

Also, Lie et al. group synthesized cobalt oxyhydroxide with oxygen vacancy (CoOOH-V_O) by electrochemical transformation of M-ZIF-67 which demonstrated superior water oxidation performance. As synthesized catalyst produced 10 $mAcm^{-2}$ of current density at very low overpotential of 170 mV with superior stability for 100 h.[22]

These reports have inspired us to develop an electrochemical method to form FeCo-LDH-x from ZIF-67 incorporating Fe(III) in the structure of the active catalysts from the electrolyte solution during the anodic reconstruction process and explored its water oxidation activity. As synthesized FeCo-LDH-x exhibited better activity than $Fe_{0.4}$Co-LDH, hydrothermally derived from ZIF-67. Electrochemically synthesized FeCo-LDH-3 required only 180 mV of overpotential to generate 50 mA cm^{-2} of current density whereas $Fe_{0.4}$Co-LDH produced the same current density at 240 mV of overpotential.

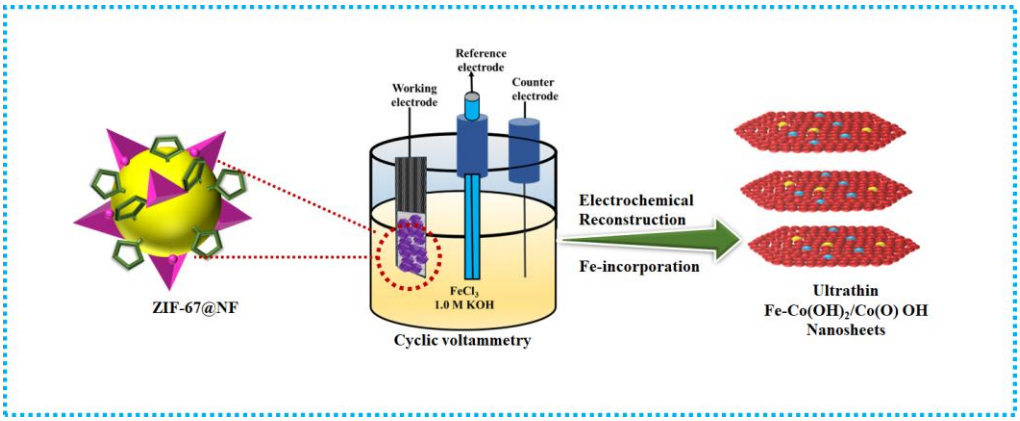

Scheme 4.1. Schematic representation showing the conversion of precatalyst ZIF-67@NF into active catalyst FeCo-LDH-3 under cyclic voltametric conditions.

4.2. Chemicals

All the chemical were used as chapter -3 except anhydrous $FeCl_3$ was used as the source of iron instead of $Fe(NO_3)_3.9H_2O$.

4.3. Instruments

Instruments have been discussed in previous chapter-3.

4.4. Experimental

4.4.1. Activation of nickel foam

Nickel foam was activated using the procedure described in Chapter 2

4.4.2. Synthesis of ZIF-67@NF

Self-supported ZIF-67 was synthesized by the method used in previous chapter-2.

4.4.3. Electrochemical reconstruction of ZIF@NF precatalyst into FeCo-LDH-x and Co-LDH

The synthesized precatalyst ZIF-67@NF was treated under cyclic voltammetric (CV) conditions using ZIF-67@NF as working electrode, Ag/AgCl as reference electrode, and Pt wire as the counter electrode. The CV was performed at a scan rate of 20 mV s^{-1} for 100 cycles in 1.0 M aqueous KOH solution. As a result, the Co-LDH (denoted as Co-LDH-3) was formed by the electrochemical reconstruction of ZIF-67@NF. For the synthesis of FeCo-LDH-5, 20 mg $FeCl_3$ was added into the 12 mL of 1.0 M aqueous KOH solution and the cyclic voltammetry was carried out for 100 cycles at the same scan rate. Interestingly, Fe was incorporated into the structure of Co-LDH during the electrochemical reconstruction by CV cycles to form FeCo-LDH active catalyst.

Similarly, different amount of $FeCl_3$ (10 mg, 15 mg, 25 mg, and 30 mg) was added into the electrolyte solution to synthesize the active FeCo-LDH-x catalysts respectively. The CV studies showed the stabilization of the CV profiles within 100 CV cycles.

4.5. Results and Discussion

4.5.1. Characterization of the Catalysts

PXRD confirmed the electrochemical reconstruction of ZIF-67 to FeCo-LDH-3 **(Figure 4.1 a)**.[23] Electronic structure and surface structure of the as synthesized catalyst FeCo-LDH-3was investigated through XPS characterization.

Table 4.1. Details of active catalysts synthesized by the electrochemical transformation of ZIF-67 and their reaction condition.

Sr. No.	Pre-catalyst	Electrochemical condition	Amount of salt	Active catalyst
1	ZIF-67@NF	100 CV-cycles, 1-2 V vs RHE	$FeCl_3$ (10 mg)	FeCo-LDH-1
2	ZIF-67@NF	100 CV-cycles, 1-2 V vs RHE	$FeCl_3$ (15 mg)	FeCo-LDH-2
3	ZIF-67@NF	100 CV-cycles, 1-2 V vs RHE	$FeCl_3$ (20 mg)	FeCo-LDH-3
4	ZIF-67@NF	100 CV-cycles 1-2 V vs RHE	$FeCl_3$ (25 mg)	FeCo-LDH-4
5	ZIF-67@NF	100 CV-cycles, 1-2 V vs RHE	$FeCl_3$ (30 mg)	FeCo-LDH-5
6	ZIF-67@NF	100 CV-cycles, 1-2 V vs RHE	$CoCl_2.6H_2O$ (20 mg)	Co-LDH-3

The Co2p XPS spectra demonstrated the coexistence of Co^{2+} and Co^{3+} in both species FeCo-LDH-3 and Co-LDH-3. The peaks obtained at the binding energies (BE) of 781.68 eV/796.96 eV were assigned to the Co^{3+} species whereas peaks at 783.30 eV and 798.97 eV were assigned to Co^{2+} species, respectively. Remaining peaks at 786.59 eV and 802.10 eV can be attributed to satellite peaks revealing the coexistence of Co^{3+} and Co^{2+} **(Figure 4.2 c)**.[24]

When compared to Co-LDH-3, the Co $2p_{3/2}$ peak of FeCo-LDH-3 had a positive shift of 0.71 eV, suggesting that the introduction of Fe into the structure of catalyst increased the positive charge density on the Co atom.[25] Furthermore, the Co 2p XPS of FeCo-LDH-3 was compared with that of $FeC_{0.4}$Co-LDH it was observed that positive shift in Co $2p_{3/2}$ peak was greater than $Fe_{0.4}$Co-LDH **(Table 4.2)**.

In the Fe 2p XPS spectra, two peaks obtained at 723.55 eV and 710.46 eV can be assigned to Fe $2p_{1/2}$ and Fe $2p_{3/2}$ with the energy separation 13.09 eV indicating the presence of Fe^{3+} as major species. [26] There was more negative shifting in Fe $2p_{1/2}$ and Fe $2p_{3/2}$ orbital spacing of Fe 2p spectra.

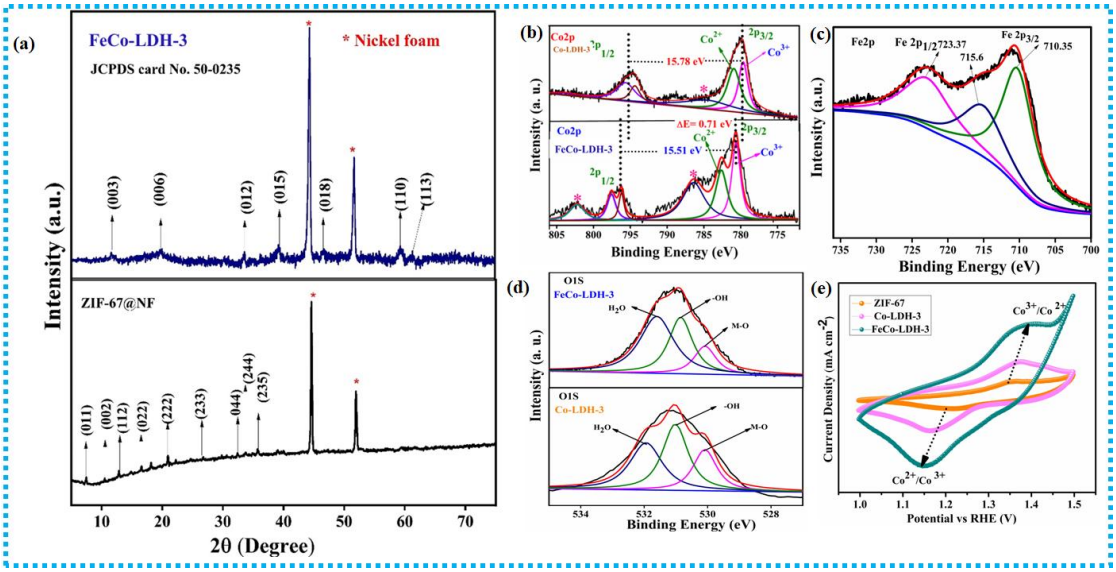

Figure 4.1. (a) The PXRD graph of ZIF-67@NF, and FeCo-LDH-3;((b) The Co 2p XPS spectra of Co-LDH-3 and FeCo-LDH-3 showing the changes in the electronic structure resulting from the incorporation of Fe(III) into the catalyst; (c) Fe 2p X-ray photoelectron spectrum of FeCo-LDH-3. The Fe2p spectrum was deconvoluted into two peaks with binding energy 723.59 eV and 710.55 eV corresponding to Fe $2p_{1/2}$ and, Fe $2p_{3/2}$; (d) The O 1s XPS of Co-LDH-3 and FeCo-LDH-3; (e) CV profiles of ZIF-67, Co-LDH-3, and FeCo-LDH-3 demonstrating the redox peaks for Co^{2+}/Co^{3+} couple.

When the Fe 2p XPS spectra was compared with that of pure Fe_2O_3, a negative shift in binding energy of Fe $2p_{3/2}$ was observed which can be attributed to reduction in the positive charge density on Fe due to the electron density draining from Co(II) to Fe(III).[27] Thus, the result obtained from XPS confirmed the strong electronic interaction between Co and Fe resulting in the redistribution of electrons **(Figure 4.2 d)**. Furthermore, these XPS results showed that stronger electronic interaction between Co and Fe in FeCo-LDH-3 than $Fe_{0.4}$Co-LDH **(Table 4.2)**.

Table 4.2 showing electronic interaction between Co and Fe in FeCo-LDH-3 and $Fe_{0.4}$Co-LDH.

Sr. No.	Catalyst	B. E. of Co^{2+} (eV)	B. E. of Co^{3+} (eV)	B. E. of Fe^{3+}	B. E. of Fe^{2+}	Amount of iron loading (w%)
1	Co-LDH-3	782.65	780.45			
2	Co-LDH	782.57	779.88			
3	FeCo-LDH-3	783.30	781.68	710.45		37.64
4	$Fe_{0.4}$Co-LDH	783.05	781.45	710.61		21.50

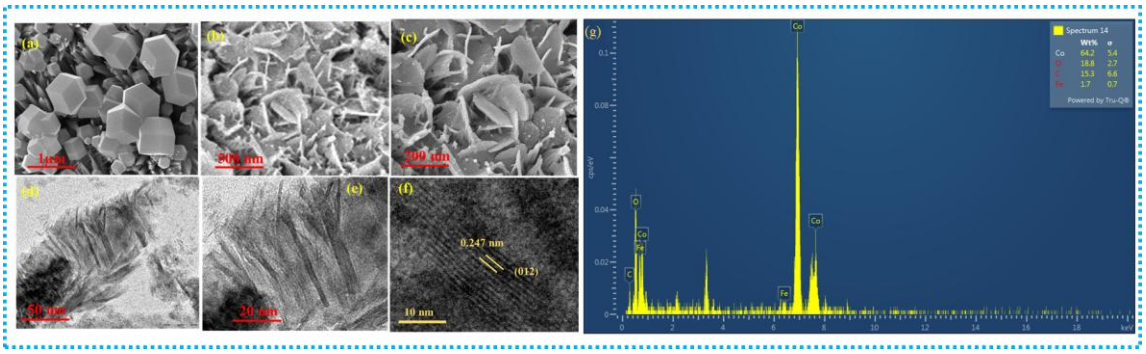

Figure 4.2. (a) SEM image of ZIF-67@NF (b-c) SEM image of FeCo-LDH-3;(d-e) TEM image showing the formation of nanosheet FeCo-LDH-3;(f) HR-TEM image of FeCo-LDH-3; (g) EDX spectrum of electrochemically derived FeCo-LDH-3 showing the existence of Co, Fe and O elements.

The O 1s XPS spectra of FeCo-LDH-3 can be deconvoluted into four peaks at 529.85 eV (O1), 530.85 eV (O2), 531.87 eV (O3), and 532.97 eV (O4) corresponding to metal-oxygen bonds (Co-O), oxygen vacancy, adsorbed -OH groups, and water molecules, respectively.[17][28] A positive shifting of 0.68 eV was observed in binding energy of -OH in the case of FeCo-LDH-3 due to introduction of Fe in comparison to Co-LDH. The electron withdrawing nature of Fe enhanced the binding energy of adsorbed -OH, resulting in a greater affinity of the Co site for adsorbed -OH **(Figure 4.2 d)**.[17]

Further, SEM studies demonstrated dodecahedral morphology of ZIF-67 was disappeared and nanosheet like morphology of FeCo-LDH-3 obtained after the electrochemical reconstruction of

ZIF-67 **(Figure 4.2 a-c)**. Corresponding elemental mapping of the catalyst confirmed the uniform distribution of Co, Fe and O in the catalyst FeCo-LDH-3 **(Figure 4.2 f)**. Furthermore, Co/Fe ratio in FeCo-LDH-3 (37.50) was greater than that of $Fe_{0.4}$Co-LDH (21.50) which indicated the controlled incorporation of Fe into the structure of Co-LDH during anodic OER process maintaining equilibrium between electrode surface and electrolyte solution containing Fe(III). TEM studies also exhibited the nanosheet like morphology of the catalyst FeCo-LDH-3 **(Figure 4.2 d-e)**. Furthermore, the high-resolution TEM (HRTEM) image shows the inter-planar distance of 0.247 nm, which can be assigned (012) plane of FeCo-LDH-3 **(Figure 4.2 f)**.[26]

4.5.2. Electrochemical activity

The OER activity of the active catalysts was assessed in 1.0 M aqueous KOH solution. The LSV profiles demonstrated a notable improve in both current density and overpotential after the ZIF-67 precatalyst was activated. Incorporating different amounts of Fe(III) electrochemically led to a broad variation in electrochemical performance. FeCo-LDH-3 exhibited best OER activity therefore we have performed all characterization of this catalysts only to get insight view. The overpotential at the current of 50 $mAcm^{-2}$ for the precatalyst ZIF-67 was determined to be 415 mV, but the active catalyst Co-LDH produced the same result at 380 mV **(Figure 4.3 a)**. Thus, the incorporation of Fe greatly increased the OER activity and it was found to be best for FeCo-LDH-3 **(Figure 4.3 b)**. OER performance of FeCo-LDH-3 was also found better than that of hydrothermally synthesized $Fe_{0.4}$Co-LDH (240 mV) and CeCo-2 (220 mV) and literature reported electrochemically derived catalysts **(Table 4.2)**.

Using the Tafel plots, the oxygen evolution kinetics of the as synthesized catalysts were evaluated. The electrochemical reconstruction was also found to result in a notable improvement in the OER reaction kinetics. In comparison to the other catalysts under study, FeCo-LDH-3 exhibited the

fastest OER kinetics, as evidenced by its lowest Tafel slope of 48 mV dec^{-1} **(Figure 4.3 c)**.

Table 4.3. The OER activities of reported LDHs compared with FeCo-LDH-3.

Sr. No.	Catalyst	Current density ($mA\ cm^{-2}$)	Overpotential (mV)	Reference
1	FeCo-LDH-3	50	180	This work
2	$Fe_{0.4}$Co-LDH@NF	50	240	[29]
3	CeCo-2	50	220	[30]
4	V-NiAC-1	50	290	[17]
5	A-$Co(OH)_2$-ZIF-L/NF	20	180	[21]
6	Ir-Ni-(Oxy)hydroxide	10	270	[31]
7	M-ZIF-67-EA	10	220	[22]
8	$FeNi(OH)_2$/NiOOH	10	270	[20]

This Tafel slope value observed for FeCo-LDH-3 (48 mV dec^{-1}) was also lower than that of $Fe_{0.4}$Co-LDH (53 mV dec^{-1}).

Moreover, all the electrochemically derived FeCo-LDH-x catalysts performed better than Co-LDH-3, according to electrochemical characterizations such as double-layer capacitance and electronic impedance spectroscopy (EIS). Electric double-layer capacitance (C_{dl}) measurements in the non-faradaic region can be used to calculate the electrochemical active surface area (ECSA) of the catalysts. FeCo-LDH-3 was observed to have the highest C_{dl} value and, consequently, the largest ECSA among all synthesized catalysts **(Figure 4.3 d)**. Furthermore, FeCo-LDH-3 demonstrated larger C_{dl} value hence greater ECSA value than $Fe_{0.4}$Co-LDH **(Table 4.4)**. According to the impedance spectra the charge transfer resistance (R_{ct}) was greatly decreased when Fe(III) was added in the solution. FeCo-LDH-3 showed the smallest R_{ct} value (0.32 Ω), which means that among all electrochemically synthesized catalysts, it has the quickest charge transfer kinetics **(Figure 4.3 e)**. It was also observed that electrochemically synthesized FeCo-LDH-3 demonstrated lower R_{ct} value (0.32 Ω) than that of hydrothermally synthesized $Fe_{0.4}$Co-

LDH (0.42 Ω).

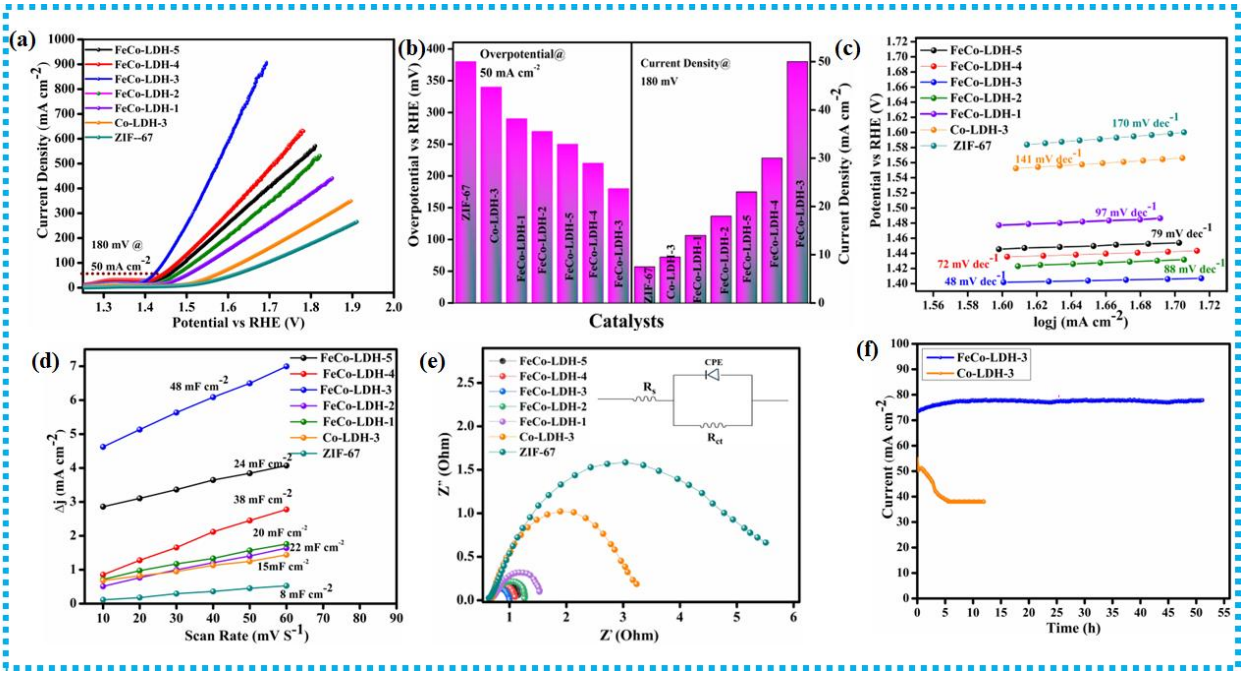

Figure 4.3. (a) LSV profile of all electrochemically derived FeCo-LDH-x shoeing the excellent performance of FeCo-LDH-3; (b) Comparison of overpotential and current density of all active catalysts (c) Tafel plots of all catalysts for OER; (d) Determination of double-layer capacitance (C_{dl}) of various synthesized catalysts by plotting (difference in current density)/2 against scan rate; (e) demonstrates Nyquist plots for all catalysts obtained from electrochemical impedance spectroscopic (EIS) measurements showing lowest charge transfer resistance for FeCo-LDH-3; (f) Chronoamperometric measurement for the oxygen evolution reaction of FeCo-LDH-3and Co-LDH-3 at 1.5 V vs RHE. The current density of Co-LDH-3 was found to decrease from the beginning due to the deactivation whereas FeCo-LDH-3 exhibited long term stability for 52 h.

We have thoroughly examined the electrochemical properties of the catalysts to understand why FeCo-LDH-3 exhibits superior water oxidation activity in comparison to other catalysts. As the current density and the redox peak area increased steadily throughout the electrochemical reconstruction, the CV curves demonstrated the activation of the precatalyst ZIF-67. The electrochemical reconstruction process to form Co- LDH-3 and FeCo-LDH-3 were reported to increase the redox peak area and it was observed that redox peak area of FeCo-LDH-3 greater than

that of ZIF-67 and Co-LDH-3 **(Figure 4.1 e)**.

Table 4.4. The OER activities of electrochemically synthesized FeCo-LDH-3, Co-LDH and hydrothermally synthesized $Fe_{0.4}$Co-LDH and Co-LDH

S. No.	Catalyst	η_{50}	C_{dl}	ECSA/mg	R_{ct} Ω
1	Co-LDH-3	380	15	133.92	2.82
2	FeCo-LDH-3	180	48	428.57	0.32
3	$Fe_{0.4}$Co-LDH	240	1.8	19.00	0.42
4	Co-LDH	415	0.59	6.70	3.43

Furthermore, stability test for the catalysts was accessed by CA. It was found that after twelve hours under CA conditions, the Co-LDH-3 lost its initial current density due to the deactivation of the catalyst. Whereas, FeCo-LDH-3 showed CA stability for 54 h at high current density without any loss of initial activity. According to this result, the addition of high valence Fe caused a sluggish deactivation process and stabilized the active catalyst, which enhanced the stability and activity of the OER **(Figure 4.3 f)**.

4.6. Conclusion

In conclusion, we have performed electrochemical incorporation of Fe(III) into the structure of ZIF-67-derived Co-LDH during OER process. Under anodic potential ZIF-67 underwent reconstruction to form ultrathin nanosheets structure which led to enhanced OER activity. The best catalyst, FeCo-LDH-3 required very low over potential of 180 mV to produce 50 mA cm^{-2} of current density with reduced Tafel slope and large electrochemical surface area. Also, FeCo-LDH-3 exhibited long-term stability for 55 h. To get insight vie of the electrochemically synthesized catalysts, in situ characterization and theoretical studies are remaining to perform.

4.7. Reference

[1] L. Gao, X. Cui, C. D. Sewell, J. Li, Z. Lin, *Chem. Soc. Rev.* **2021**, *50*, 8428.

[2] B. Singh, A. Singh, A. Yadav, A. Indra, *Coord. Chem. Rev.* **2021**, *447*, 214144.

[3] M. Ding, J. Chen, M. Jiang, X. Zhang, G. Wang, *J. Mater. Chem. A* **2019**, *7*, 14163.

[4] K. Yue, J. Liu, C. Xia, K. Zhan, P. Wang, X. Wang, Y. Yan, B. Y. Xia, *Mater. Chem. Front.* **2021**, *5*, 7191.

[5] B. Zhang, Z. Qi, Z. Wu, Y. H. Lui, T. H. Kim, X. Tang, L. Zhou, W. Huang, S. Hu, *ACS Energy Lett.* **2019**, *4*, 328.

[6] J. Morales-Vidal, R. García-Muelas, M. A. Ortuño, *Catal. Sci. Technol.* **2021**, *11*, 1443.

[7] K. Ge, S. Sun, Y. Zhao, K. Yang, S. Wang, Z. Zhang, J. Cao, Y. Yang, Y. Zhang, M. Pan, L. Zhu, *Angew. Chem., Int. Ed*. **2021**, 60, 12097.

[8] S. Zhao, C. Tan, C. T. He, P. An, F. Xie, S. Jiang, Y. Zhu, K. H. Wu, B. Zhang, H. Li, J. Zhang, Y. Chen, S. Liu, J. Dong, Z. Tang, *Nat. Energy* **2020**, *5*, 881.

[9] J. Zhou, Y. Wang, X. Su, S. Gu, R. Liu, Y. Huang, S. Yan, J. Li, S. Zhang, *Energy Environ. Sci.* **2019**, *12*, 739.

[10] M. Zhang, W. Xu, T. Li, H. Zhu, Y. Zheng, *Inorg. Chem.* **2020**, *59*, 15467.

[11] L. Huang, G. Gao, H. Zhang, J. Chen, Y. Fang, S. Dong, *Nano Energy* **2020**, *68*, 104296.

[12] H. Yin, L. Jiang, P. Liu, M. Al-Mamun, Y. Wang, Y. L. Zhong, H. Yang, D. Wang, Z. Tang, H. Zhao, *Nano Res.* **2018**, *11*, 3959.

[13] N. Yao, Z. Fan, R. Meng, H. Jia, W. Luo, *Chem. Eng. J.* **2021**, *408*, 127319.

[14] X. Su, Y. Wang, J. Zhou, S. Gu, J. Li, S. Zhang, *J. Am. Chem. Soc.* **2018**, *140*, 11286.

[15] Y. Liu, C. Wang, S. Ju, M. Li, A. Yuan, G. Zhu, *Prog. Nat. Sci. Mater. Int.* **2020**, *30*, 185.

[16] F. Wu, X. Guo, G. Hao, Y. Hu, W. Jiang, *Nanoscale*, **2019**, 11, 14785.

[17] B. Singh, Y. C. Huang, A. Priyadarsini, P. Mannu, S. Dey, G. K. Lahiri, B. S. Mallik, C. L. Dong, A. Indra, *J. Mater. Chem. A* **2023**, *11*, 15906.

[18] J. Tian, F. Jiang, D. Yuan, L. Zhang, Q. Chen, M. Hong, Angew. Chem., Int. Ed., 2020, 59, 13101.

[19] X. Ling, F. Du, Y. Zhang, Y. Shen, W. Gao, B. Zhou, Z. Wang, G. Li, T. Li, Q. Shen, Y. Xiong, X. Wang, Y. Zhou, Z. Zou, *J. Mater. Chem. A* **2021**, *9*, 13271.

[20] B. Singh, O. Prakash, P. Maiti, P. W. Menezes, A. Indra, *Chem. Commun.* **2020**, *56*, 15036.

[21] J. Ding, T. Fan, K. Shen, Y. Li, *Appl. Catal. B Environ.* **2021**, *292*, 120174.

[22] Z. Lei, X. Jin, J. Li, Y. Liu, J. Liu, S. Jiao, R. Cao, *J. Energy Chem.* **2022**, *65*, 505.

[23] S. Shahparast, K. Asadpour-Zeynali, *ACS Omega* **2023**, *8*, 1702.

[24] B. Singh, A. Indra, *Dalt. Trans.* **2021**, *50*, 2359.

[25] B. Singh, A. K. Patel, A. Indra, *Mater. Today Chem.* **2022**, *25*, 100930.

[26] J. Zhao, X. R. Wang, F. W. Chen, C. He, X. J. Wang, Y. P. Li, R. H. Liu, X. M. Chen, Y. J. Hao, M. Yang, F. T. Li, *Inorg. Chem. Front.* **2020**, *7*, 737.

[27] P. Kaspar, D. Sobola, R. Dallaev, S. Ramazanov, A. Nebojsa, S. Rezaee, L. Grmela, *Appl. Surf. Sci.* **2019**, *493*, 673.

[28] H. Liang, H. Jia, T. Lin, Z. Wang, C. Li, S. Chen, J. Qi, J. Cao, W. Fei, J. Feng, *J. Colloid Interface Sci.* **2019**, *554*, 59.

[29] P. Maurya, V. Vyas, A. N. Singh, A. Indra, *Chem. Commun.* **2023**, 7200.

[30] P. Maurya, T. Ansari, A. Indra, *Chem. Commun.* **2023**, *59*, 13359.

[31] J. Liu, J. Xiao, Z. Wang, H. Yuan, Z. Lu, B. Luo, E. Tian, G. I. N. Waterhouse, *ACS Catal.* **2021**, *11*, 5386.